Editors' Suggestion

Oxygen-Migration-Based Spintronic Device Emulating a Biological Synapse

Rahul Mishra, Dushyant Kumar, and Hyunsoo Yang*
Department of Electrical and Computer Engineering, National University of Singapore, 117576 Singapore

(Received 1 February 2019; revised manuscript received 8 April 2019; published 23 May 2019)

Electronic emulation of the biological synapse, which is the memory and learning element of the brain, is an important step towards the realization of brain-inspired computing systems. However, a complementary metal-oxide-semiconductor–based implementation of a synapse is not scalable due to the power and area inefficiency. It is therefore essential to develop alternative material and device concepts that can mimic the maximum number of synaptic functionalities in an energy-efficient way. Here, we demonstrate a nanosized energy-efficient three-terminal artificial synapse, with a separate read and write path, based on a magnetic material (Co) that could generate both positive and negative synaptic outputs. The Co magnetization, which is representative of the synaptic weight, is modulated in an energy-efficient way by using an electric field to transport oxygen ions in and out of the Co layer. A wide range of synaptic functions such as synaptic potentiation and depression, spike magnitude, rate, and timing-dependent plasticity, and the transition from short-term to long-term plasticity are demonstrated. Our results suggest the viability of a spintronic synapse in neuromorphic computing.

DOI: 10.1103/PhysRevApplied.11.054065

I. INTRODUCTION

Electronic emulation of the biological synapse, which is the memory and learning element of the brain, is an important step towards brain-inspired computing systems. However, a complementary metal-oxide-semiconductor–based synapse is not scalable due to the power and area inefficiency. Materials displaying memristorlike [1] behaviors have been widely studied for realizing potential synaptic devices [2–8]. Memristor-based synapses are two-terminal devices, which can be programmed with variable conductances by passing a current through them [9,10]. The different conductance states of a memristor are considered as a representation of the distinct synaptic weights. However, there are two inherent limitations in the memristor-based synaptic devices. The first and a less serious limitation is the shared read and write paths. While a two-terminal device with a common read and write channel promises a densely packed architecture, it comes at the cost of an increased read and write latency in addition to the energy-expensive writing and the fluctuation of the programmed synaptic weights during the read operation. Despite the fact that this fluctuation of synaptic weights can be kept at a minimum by reducing the read current magnitude, it inadvertently leads to an increased read error rate.

The second and the more critical limitation of memristor synapse, which has been somewhat overlooked by the researchers until now, is the ineffectiveness of a memristor to be programmed with a negative synaptic weight, which could appropriately yield an inhibitory postsynaptic potential. In a human brain, a synapse could produce either an excitatory potential (positive weight) or an inhibitory potential (negative weight) in order to increase or decrease the membrane potential of the postsynaptic neuron, respectively. However, a memristor-based synapse can only emulate a positive weight because a positive potential difference across it would always generate a positive current spike due to the scalar nature of the conductance. This positive current spike is incapable of decreasing a postsynaptic neuron potential and can only continually increase the postsynaptic potential by either a smaller or a larger amount, depending on the magnitude of the memristor conductance or the synaptic weight. Due to the above drawbacks, it would be difficult to realize a true brain-inspired neuromorphic system using memristors. It is therefore critical to come up with alternative materials and device concepts in order to emulate a true biological synapse.

Spintronic devices, which rely on the spin degree of freedom of electrons, are considered as a viable replacement of charge-based computing and memory elements [11–13], promising nonvolatility, low power consumption, and faster speed. Recent demonstrations [6,14–16] have aroused research enthusiasm towards extending spin devices to the field of neuromorphic computing [14,17,18]. While the neural functionalities have been implemented to some extent using the spin elements [6], the synaptic implementation is mostly limited to the demonstration of multilevel programming capability [15,16].

*eleyang@nus.edu.sg

In this paper, we propose a spintronic-based artificial synapse, which not only has a multilevel programming potential but could also mimic a wide range of synaptic functionalities, such as potentiation, depression, spike magnitude, rate, and timing-dependent plasticity, and transition from short-term plasticity (STP) to long-term plasticity (LTP). Furthermore, there is separation of the read and write paths and a capability to be programmed with a negative synaptic weight, thereby, overcoming the downsides of memristor-based synapses [2–7]. A magnetic layer of Co on top of Pt acts as the main functional layer of our synapse and a GdO_x gate is used for programming its weight. The oxygen-ion (O^{2-}) migration under the application of an electric field on GdO_x assists in accomplishing various synaptic functions. Our results demonstrate the feasibility of a magnetic synapse for future brain-inspired computing.

II. RESULTS AND DISCUSSION

First, we explain the design of our device (magnetic synapse) and answer three important questions: (i) how the magnetic device serves as a potential synapse, (ii) how the separation of read and write paths is achieved, and (iii) how the device is programmed with weights of opposite polarity. The design of the magnetic synapse consists of an ultrathin magnetic layer of Co(0.8 nm) with perpendicular magnetic anisotropy (PMA), which is deposited on top of 1.5-nm-thick Pt using sputter. The Pt/Co stack is capped with an approximately 3-nm thin oxide layer of GdO_x. The GdO_x layer is deposited by reactive sputtering of Gd in oxygen partial pressure of 0.07 mTorr. Figure 1(a) shows a schematic of the film structure. The film stack is then fabricated in the form of a Hall bar of width 500 nm using electron-beam lithography and subsequent ion milling. The Hall cross is then covered with an approximately 20-nm-thick GdO_x gate oxide as shown in Fig. 1(b). In the final step of device fabrication, the Hall cross and the gate oxide are covered with Cr(10 nm)/Au(80 nm) electrodes.

The weight of the magnetic synapse is defined using the measure of net Co magnetization. An effective way to quantify the Co magnetization is to evaluate the anomalous Hall resistance (R_{AHE}), which is proportional to the net out-of-plane magnetization [19]. The different values of R_{AHE} correspond to the distinct weights of the magnetic synapse and the anomalous Hall voltage (V_{AHE}) represents the weighted synaptic output signal, which can be passed as an input to the postsynaptic neuron. The programming of the synaptic weights is achieved by modulating the Co magnetization by applying the top gate voltage (V_g) [20]. The application of a negative gate voltage as shown in Fig. 1(c) drives the O^{2-} from GdO_x into the Co layer [20–25] and oxidizes the Co atoms. The oxidized Co atoms (CoO) are paramagnetic at room temperature, which result in the reduction of the overall saturation magnetization of

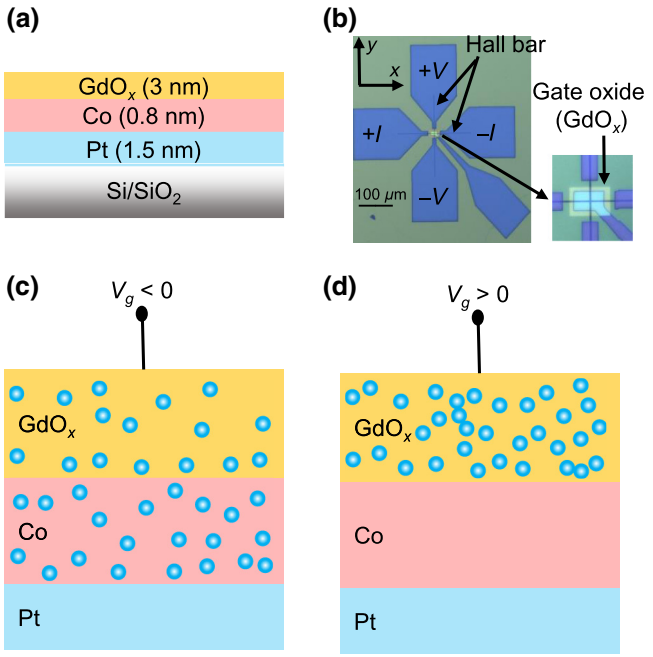

FIG. 1. (a) Schematic of the film structure. (b) Schematic of the Hall bar before electrode deposition. Enlarged view of the Hall cross is shown in the inset. (c) State of the magnetic synapse under the application of negative gate voltage (V_g). Blue spheres represent oxygen ions. (d) State of the magnetic synapse under the application of positive gate voltage.

the Co layer. On the other hand, on applying a positive V_g as shown in Fig. 1(d), the O^{2-} migrates back from the Co layer into the GdO_x layer. This reduces the CoO into Co resulting in increasing the magnetization of the Co layer. In our magnetic synapse, therefore, there is a clear separation of the read and write path as the reading of the device is carried out by passing currents through the main channel and measuring the V_{AHE} [see connections in Fig. 1(b)], whereas the writing of the synaptic weights is achieved via applying a gate voltage on top of the device.

Finally, the polarity of the programmed weight or the R_{AHE} is determined by the out-of-plane direction of the Co magnetization [19]. For a current passing along the $+x$ direction [axes labeled in Fig. 1(b)], if R_{AHE} is measured across the $+y$ direction, then $+z$ and z directions of Co magnetization results in positive and negative R_{AHE}, respectively. Accordingly, the polarity of synaptic weights can be toggled by switching the magnetization direction by utilizing the current-induced spin torque from the underlying Pt layer [26,27].

A. Potentiation and depression

We now demonstrate the emulation of basic synaptic functions like potentiation, depression, spike magnitude, rate, and, timing-dependent plasticity, using the proposed magnetic synapse. Apart from mimicking the synaptic

functions, the magnetic synapse also displays a basic learning behavior, which transforms a STP to LTP similar to a human brain. The most important aspect of a biological synapse is its plasticity. A synaptic plasticity refers to the ability of a synapse to dynamically modulate its weight. This modulation occurs in response to the activity of the pre and postsynaptic neurons [28–30]. A synapse in the brain strengthens when it receives a positive stimulation and this strengthening or increase in its weight is referred to as synaptic potentiation. To demonstrate synaptic potentiation, we start with an initial magnetic state with $R_{AHE} = 3.1\ \Omega$ for which PMA is still maintained. For all the measurements, square V_g pulses with a slew rate of 30 V/ms are applied. As shown in Fig. 2(a), when V_g pulses of +10 V and 50 ms duration (rise-fall time approximately 333 μs) are applied on the magnetic synapse, an increase in R_{AHE} is observed, which corresponds to an increase of the synaptic weight. The increase of R_{AHE} is due to the migration of O^{2-} from Co into the GdO_x gate under the effect of electric fields [Fig. 1(d)]. The magnetic synapse reaches 100% of its maximum weight on application of 60 positive V_g pulses. In effect, we demonstrate the characteristics of synaptic potentiation in the magnetic synapse with the data points in Fig. 2(a) representing the various values of weight, which the magnetic synapse could attain. It is also important to note that the weight of the magnetic synapse can be programmed to have negative values by reversing the direction of Co magnetization, as shown in Fig. 2(a).

A synaptic depression signifies the weakening or reduction of the synaptic weight on receiving negative stimulation. In order to demonstrate the synaptic depression in the magnetic device, 50-ms-long V_g pulses of −10 V are subsequently applied on the device and it is observed that the R_{AHE} value or the synaptic weight reduces after each pulse. The negative V_g pulses drive the O^{2-} from GdO_x into the Co [Fig. 1(c)], thereby reducing its saturation magnetization (M_s) by means of oxidation. The synaptic weight can thus be programmed back to its initial value by applying about 30 negative pulses. It should be noted that for our device the synaptic depression is more efficient as it requires around 30 pulses, which is half the number of pulses required (60 pulses) for synaptic potentiation. This is possibly because of the enhancement in the back migration of O^{2-} into Co by an additional process of diffusion, which favors movement of O^{2-} from GdO_x into Co than the other way around. The fast depression and slow potentiation behavior in our device is similar to the functioning of a human brain where synapse strengthening or memory formation requires a longer time and stronger stimulation in an untrained brain. It should also be noted that due to the stochastic nature of our device, a different number of V_g pulses is required in different potentiation and depression cycles, in order to attain a particular device state. This stochastic behavior is primarily due to the random activation of new oxidation and reduction pathways during each cycle [9].

B. Spike-magnitude dependence

Another feature of the biological synapse is that its strengthening rate is proportional to the magnitude of the applied stimulation. A stimulation of larger magnitude would produce a larger change in synaptic weight compared to a stimulation of smaller magnitude [2,4,6,31]. When our magnetic synapse is stimulated with V_g pulses of various magnitudes, the percentage change in synaptic weight is found to be proportional to the pulse amplitude. For instance, 30 sequential V_g pulses of +10 V magnitude result in only a 24% increase in the synaptic weight compared to a much larger change of 53% induced by +14 V V_g pulses, as shown in Fig. 2(b). Furthermore, a reduction

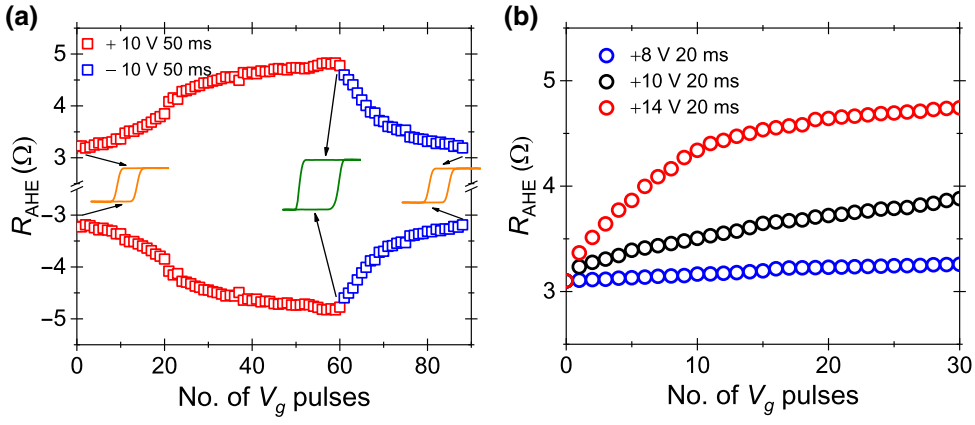

FIG. 2. (a) Potentiation and depression of the magnetic synapse using positive and negative gate-voltage pulses. Magnetic hysteresis loops for the magnetic state with minimum and maximum magnetic weights are also shown. The Co magnetization is switched between the up and down state to emulate positive and negative synaptic weight. (b) Dependence of the anomalous Hall resistance (R_{AHE}) or the synaptic weight on the magnitude of the V_g pulse.

in the V_g pulse magnitude to +8 V results in a meager modulation of 5%. The spike-magnitude dependence of the magnetic synaptic weight is due to proportionality between the O^{2-} migration rate and the applied electric field.

C. Spike-timing dependence

The synaptic plasticity depends not only on the magnitude and polarity of the action potential that it receives but on the temporal relation between the action potentials [29,30]. A biological synapse that is stimulated frequently shows a larger modulation in its weight compared to a synapse that is not simulated often [2,4,29,30]. This behavior is referred to as the spike-rate-dependent plasticity. In order to test the spike-rate-dependent plasticity of our magnetic synapse, trains of V_g pulses of fixed magnitude (+5 V) but variable delay time are applied on the device. Before application of each V_g pulse train, the synaptic weight is set to its minimum value and then the evolution of synaptic weight is monitored while the pulses are applied. The synaptic weight is monitored after every 20 pulse-application events. As shown in Fig. 3(a), for a larger time delay between subsequent pulses, the synaptic weight increases by a smaller amount compared to the case for which the time delay is shorter. For example, a train of 1400 V_g pulses of magnitude +5 V and a time delay of 10 ms results in a 55% modulation of synaptic weight. This modulation is around four times higher compared to the case when a pulse train of similar magnitude and duration but with a time delay of 400 ms is applied on the device.

Another temporal relation between the different stimulations that affects a synaptic plasticity is a spike-timing-dependent plasticity (STDP) [29,30,32]. STDP results in a weight modulation whose magnitude depends on the relative arrival of pre and postsynaptic spikes, $\Delta t_{\text{pre-post}}$. If the presynaptic spike is followed by the postsynaptic spike ($\Delta t_{\text{pre-post}} > 0$), the synaptic weight increases signifying stronger causality. On the other hand, if the presynaptic spike occurs after the postsynaptic spike ($\Delta t_{\text{pre-post}} < 0$), the resultant synaptic weight decreases indicating weaker causality. Furthermore, if the time difference between the pre and postsynaptic spike is large, the weight modulation is small and conversely a smaller time difference results in a larger weight modulation. In previous works, the input signals used for demonstrating the STDP behavior were implemented using a variety of methods. These methods included the use of overlapping pre and postsynaptic waveforms [33,34], nonoverlapping pre and postsynaptic waveforms [4,7], overlapping asymmetric waveforms [35], single equivalent waveform [6], and conversion of pulse-timing information to pulse-width information [2,36].

In our work, we use the method of converting pulse-timing ($\Delta t_{\text{pre-post}}$) information into pulse-width (Δw_{pulse}) information and the resultant pulses are applied to the magnetic synapse. The exponential relationship between the pulse timing and pulse width (evaluated in Ref. [2]) is used to map the two timing pieces of information. Specifically, using the transfer function $\Delta w_{\text{pulse}} = Ae^{-\Delta t_{\text{pre-post}}/t_0}$, the $\Delta t_{\text{pre-post}}$ is converted into Δw_{pulse}. The values of constants A and t_0 are chosen such that Δw_{pulse} is greater than 10 ms. Subsequently, potentiating and depressing voltage pulses of a magnitude of +10 V and −10 V, respectively, are applied in order to change the synaptic weight, ΔR_{AHE}. The duration and width of the pulses (Δw_{pulse}) is selected from the Δw_{pulse} versus $\Delta t_{\text{pre-post}}$ mapping. Figure 3(b) shows ΔR_{AHE} (%) obtained using the expression $\Delta R_{\text{AHE}}(\%) = 100 \times (R_{\text{AHE}}^{\text{final}} - R_{\text{AHE}}^{\text{initial}})/R_{\text{AHE}}^{\text{initial}}$, as a function of $\Delta t_{\text{pre-post}}$. Prior to the individual potentiating or depressing pulse application, $R_{\text{AHE}}^{\text{initial}}$ is set to the minimum or maximum value of R_{AHE}, respectively. It is observed that a smaller value of $\Delta t_{\text{pre-post}}$ results in a larger modulation of ΔR_{AHE} in comparison to a larger value of $\Delta t_{\text{pre-post}}$. As shown in

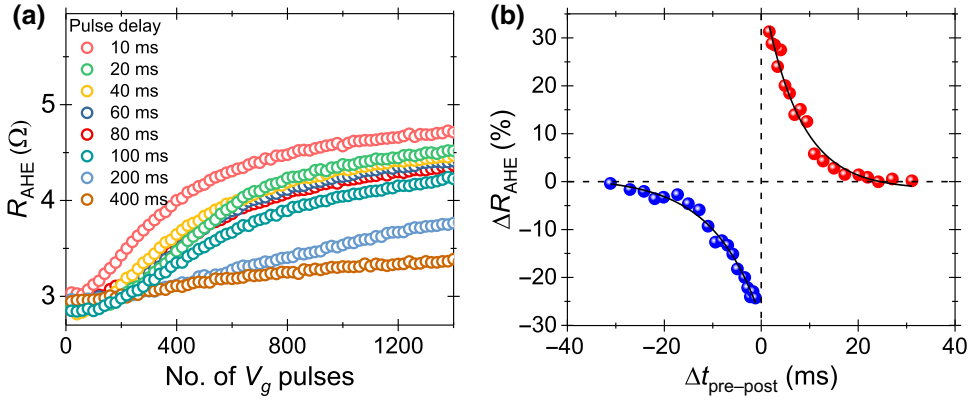

FIG. 3. (a) Evolution of the anomalous Hall resistance or the weight of the magnetic synapse under the application of consecutive gate-voltage pulse of +5 V magnitude and 50 ms duration. Various curves represent the device evolution for the different values of time delay between each pulse. Readings are taken after every 20 pulse-application events. (b) Dependence of the synaptic weight modulation on the relative timing of the pre and postsynaptic pulses. Solid lines represent an exponential fit.

Fig. 3(b), the resulting curve of ΔR_{AHE} versus $\Delta t_{\mathrm{pre-post}}$ follows an exponential waveform, which is similar to the STDP behavior of a biological synapse. Qualitatively similar results are obtained when the STDP behavior is emulated by applying an equivalent combination of the pre and postsynaptic waveform.

D. Learning and forgetting behavior

In general, a memory can be categorized into a short-term or long-term memory depending on the time scale of retention of the synaptic weight [37–40]. The behavior of the synapse to retain the potentiated state for a very short time is STP. In order to evaluate STP of our magnetic synapse, 100-ms-long V_g pulses of +10 V magnitude are first applied on the magnetic synapse until it is potentiated to the maximum R_{AHE} or weight. Subsequently, the state of the device is monitored after setting V_g to 0 V and it is observed that the R_{AHE} slowly decreases [see Fig. 4(a)]. The retention of the potentiated state for a short amount of time indicates the STP of the magnetic synapse, which occurs because the fully potentiated state (100% R_{AHE}) is metastable. Once the electric field is removed after driving the device in the maximum R_{AHE} or weight state, the O^{2-} starts diffusing back from GdO_x into Co thereby reducing the synaptic weight.

Furthermore, the potentiation of the device is performed several times and the pulse stimulation is stopped when the weight reaches its maximum value. After each cycle of potentiation, the reproducible STP of the magnetic synapse is observed, as shown in Fig. 4(b). The decaying R_{AHE} curves represent the forgetting behavior of the brain and are fitted with the customized Kohlrausch equation, which simulates the forgetting function [40]

$$R_{\mathrm{AHE}}(t) = R_{\mathrm{AHE}}(t_\infty) + Ce^{-t/\tau}, \qquad (1)$$

where C is the exponential constant and τ is the relaxation time constant that signifies the forgetting or relaxation rate. After fitting the forgetting curves in Fig. 4(b) with Eq. (1), we obtain an average τ of 210 s for the magnetic synapse. The exponential decay curve of the synaptic weight resembles the solution of the one-dimensional diffusion equation for microparticles that also follows an exponential law. This similarity confirms that the STP in our magnetic synapse is due to the back diffusion of O^{2-} from GdO_x.

E. STP to LTP

When a potentiated synaptic weight is retained for a relatively longer time, it is referred to as a LTP. In the brain, the STP of a synapse is converted into an LTP by repeated training. For our magnetic device the repeated training is emulated by applying V_g pulses (+10 V, width of 100 ms) after 100% potentiation is achieved. Interestingly, it is found that the relaxation time of maximum potentiation increases on increasing the number of training pulses, N. Here, N refers to the number of pulses applied after the device reaches its maximum weight. Figures 5(a)–5(d) show the forgetting or relaxation curve for the device after applying an increasing number of training pulses. For the cases without any training [Fig. 4(b)] or with a minimum amount of training [Fig. 5(a)], the synapse displays predominantly STP with a faster relaxing rate. On the other hand, when the number of training pulses increases, the relaxation rate keeps on decreasing [Figs. 5(a)–5(d)] because of the reduction in the back diffusion of O^{2-}. The value of τ is extracted by fitting the relaxation curves with Eq. (1) and it increases with the repetition number of the training pulses, as shown in Fig. 5(e). The increasing trend of τ with respect to N suggests the feasibility of the magnetic synapse to transit from a STP to LTP. This memory retention behavior by the magnetic

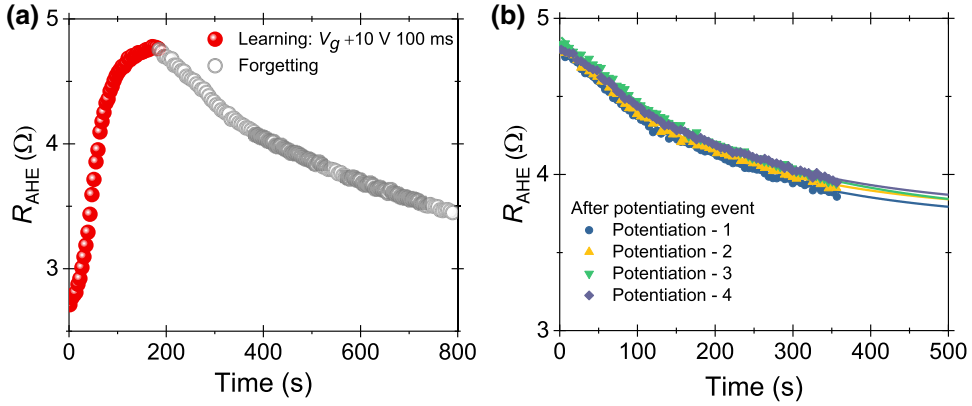

FIG. 4. (a) Learning and forgetting curve of the magnetic synapse. Gate voltage is set to 0 V while measuring the anomalous Hall resistance during the forgetting or relaxation process. (b) Forgetting or relaxation process after consecutive learning events that do not include any training step. Solid lines represent fits using Eq. (1).

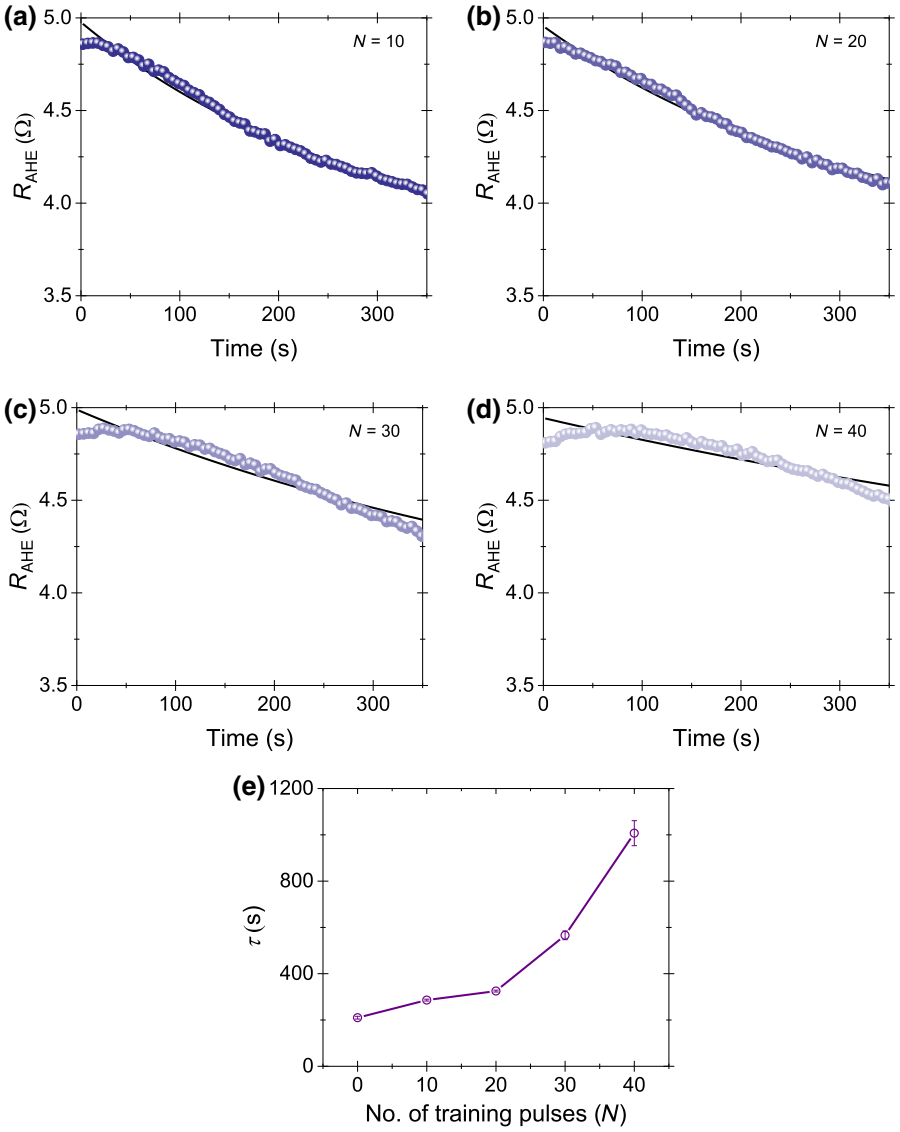

FIG. 5. (a)–(d) Forgetting or relaxation curve of the magnetic synapse after applying a different number (N) of training pulses. Training pulses are applied after setting the magnetic synapse to its maximum weight. Solid lines represent the fits using Eq. (1). (e) Relaxation time as a function of the number of training pulses.

device closely resembles the functioning of the human brain.

III. CONCLUSION AND SUMMARY

In comparison to the two-terminal memristor-based synapses, which are being actively pursued [9,41], the three-terminal magnetic synapse offers the advantage of a separate low-energy write path. The advantage of a separate write path is the minimum disturbance of the synaptic weight during the read operation, which is unavoidable in the two-terminal configuration. Another advantage of three-terminal operation is the low-energy consumption during weight programming. Since the weight of magnetic synapse is modulated from the top gate oxide, which has nominal resistance value in the range of GΩ, the resulting writing current is very low (nA range). Consequently, there is low power consumption during the potentiation and depression of weight. In contrast, the memristive synapses typically have a resistance in the range of kΩ to MΩ [41], with an even lower base value when operating at maximum weight. This results in comparatively larger power consumption during their write operation.

The state-of-the-art memristive synapses can be written with pulse duration ranging from tens of ns [41,42] to hundreds of μs [41,43]. The future work on magnetic synapse should involve reduction in the writing pulse width, which is in the range of ms for the reported device. This can be achieved by engineering the gate oxide material and its thickness. It has been already shown that by engineering the morphology and thickness of the gate oxide and gate electrode, magnetic modulation can be achieved using μs pulses for a Co/GdO_x heterostructure [22]. The magnetic synapse also needs to be improved in terms of the dynamic range of the programmable weight, which for the various memristor synapses is in between 2 and 10^5 (the ratio of

the maximum to minimum weight) [44,45]. Selecting a magnetic material with a large value of R_{AHE} would help to bring this improvement.

In summary, we demonstrate a Pt/Co/GdO_x-based nanometer-sized magnetic synapse. The magnetic synapse has separation of the read and write path. The weight of the synapse can take both positive and negative values to generate both excitatory and inhibitory synaptic potential. The weight of the synapse is potentiated or depressed in an energy-efficient way by electric fields through GdO_x, which results in the migration of oxygen ion between the GdO_x and Co layer. Fundamental synaptic functions like potentiation, depression, spike magnitude, rate, and timing-dependent plasticity are demonstrated. Repeated training of the synapse results in transition from short-term plasticity to long-term plasticity, which is one of the fundamental feature of biological memory. Magnetic synapse is a conjunction of two fields, namely the spintronics and neuromorphic computing, enabling brain-inspired computing.

ACKNOWLEDGMENTS

This work was partially supported by the National Research Foundation (NRF), Prime Minister's Office, Singapore, under Competitive Research Programme (NRFCRP12-2013-01) and SpOT-LITE programme (A*STAR Grant No. A18A6b0057) through RIE2020 funds from Singapore.

[1] D. B. Strukov, G. S. Snider, D. R. Stewart, and R. S. Williams, The missing memristor found, Nature **453**, 80 (2008).

[2] S. H. Jo, T. Chang, I. Ebong, B. B. Bhadviya, P. Mazumder, and W. Lu, Nanoscale memristor device as synapse in neuromorphic systems, Nano Lett. **10**, 1297 (2010).

[3] M. Prezioso, F. Merrikh-Bayat, B. D. Hoskins, G. C. Adam, K. K. Likharev, and D. B. Strukov, Training and operation of an integrated neuromorphic network based on metal-oxide memristors, Nature **521**, 61 (2015).

[4] Z. Q. Wang, H. Y. Xu, X. H. Li, H. Yu, Y. C. Liu, and X. J. Zhu, Synaptic learning and memory functions achieved using oxygen ion migration/diffusion in an amorphous InGaZnO memristor, Adv. Funct. Mater. **22**, 2759 (2012).

[5] T. Chang, S.-H. Jo, and W. Lu, Short-term memory to long-term memory transition in a nanoscale memristor, ACS Nano **5**, 7669 (2011).

[6] P. Krzysteczko, J. Münchenberger, M. Schäfers, G. Reiss, and A. Thomas, The memristive magnetic tunnel junction as a nanoscopic synapse-neuron system, Adv. Mater. **24**, 762 (2012).

[7] C. Du, W. Ma, T. Chang, P. Sheridan, and W. D. Lu, Biorealistic implementation of synaptic functions with oxide memristors through internal ionic dynamics, Adv. Funct. Mater. **25**, 4290 (2015).

[8] X. Yan, J. Zhao, S. Liu, Z. Zhou, Q. Liu, J. Chen, and X. Y. Liu, Memristor with Ag-cluster-doped TiO_2 films as artificial synapse for neuroinspired computing, Adv. Funct. Mater. **28**, 1705320 (2018).

[9] J. J. Yang, D. B. Strukov, and D. R. Stewart, Memristive devices for computing, Nat. Nanotechnol. **8**, 13 (2012).

[10] D. S. Jeong, K. M. Kim, S. Kim, B. J. Choi, and C. S. Hwang, Neuromorphic computing: Memristors for energy-efficient new computing paradigms, Adv. Electron. Mater. **2**, 1600090 (2016).

[11] S. Manipatruni, D. E. Nikonov, and I. A. Young, Beyond CMOS computing with spin and polarization, Nat. Phys. **14**, 338 (2018).

[12] F. Pulizzi, Spintronics, Nat. Mater. **11**, 367 (2012).

[13] I. Žutić, J. Fabian, and S. D. Sarma, Spintronics: Fundamentals and applications, Rev. Mod. Phys. **76**, 323 (2004).

[14] J. Torrejon, M. Riou, F. A. Araujo, S. Tsunegi, G. Khalsa, D. Querlioz, P. Bortolotti, V. Cros, K. Yakushiji, A. Fukushima, H. Kubota, S. Yuasa, M. D. Stiles, and J. Grollier, Neuromorphic computing with nanoscale spintronic oscillators, Nature **547**, 428 (2017).

[15] S. Lequeux, J. Sampaio, V. Cros, K. Yakushiji, A. Fukushima, R. Matsumoto, H. Kubota, S. Yuasa, and J. Grollier, A magnetic synapse: Multilevel spin-torque memristor with perpendicular anisotropy, Sci. Rep. **6**, 31510 (2016).

[16] W. A. Borders, H. Akima, S. Fukami, S. Moriya, S. Kurihara, Y. Horio, S. Sato, and H. Ohno, Analogue spin–orbit torque device for artificial-neural-network-based associative memory operation, Appl. Phys. Exp. **10**, 013007 (2017).

[17] N. Locatelli, V. Cros, and J. Grollier, Spin-torque building blocks, Nat. Mater. **13**, 11 (2013).

[18] A. Sengupta, Y. Shim, and K. Roy, Proposal for an all-spin artificial neural network: Emulating neural and synaptic functionalities through domain wall motion in ferromagnets, IEEE Trans. Biomed. Circ. Syst. **10**, 1152 (2016).

[19] N. Nagaosa, J. Sinova, S. Onoda, A. H. MacDonald, and N. P. Ong, Anomalous Hall effect, Rev. Mod. Phys. **82**, 1539 (2010).

[20] C. Bi, C. Bi, Y. Liu, T. Newhouse-Illige, M. Xu, M. Rosales, J. W. Freeland, O. Mryasov, S. Zhang, S. G. E. te Velthuis, and W. G. Wang, Reversible Control of Co Magnetism by Voltage-Induced Oxidation, Phys. Rev. Lett. **113**, 267202 (2014).

[21] M. Huang, A. J. Tan, M. Mann, U. Bauer, R. Ouedraogo, and G. S. D. Beach, Three-terminal resistive switch based on metal/metal oxide redox reactions, Sci. Rep. **7**, 7452 (2017).

[22] U. Bauer, L. Yao, A. J. Tan, P. Agrawal, S. Emori, H. L. Tuller, S. van Dijken, and G. S. D. Beach, Magneto-ionic control of interfacial magnetism, Nat. Mater. **14**, 174 (2014).

[23] U. Bauer, S. Emori, and G. S. D. Beach, Voltage-controlled domain wall traps in ferromagnetic nanowires, Nat. Nanotechnol. **8**, 411 (2013).

[24] C. Bi, M. Xu, H. Almasi, M. Rosales, and W. Wang, Metal based nonvolatile field-effect transistors, Adv. Func. Mater. **26**, 3490 (2016).

[25] R. Mishra, F. Mahfouzi, D. Kumar, K. Cai, M. Chen, X. Qiu, N. Kioussis, and H. Yang, Electric-field control of spin accumulation direction for spin-orbit torques, Nat. Commun. **10**, 248 (2019).

[26] I. M. Miron, K. Garello, G. Gaudin, P.-J. Zermatten, M. V. Costache, S. Auffret, S. Bandiera, B. Rodmacq, A. Schuhl, and P. Gambardella, Perpendicular switching of a single ferromagnetic layer induced by in-plane current injection, Nature **476**, 189 (2011).

[27] L. Liu, C.-F. Pai, Y. Li, H. W. Tseng, D. C. Ralph, and R. A. Buhrman, Spin-torque switching with the giant spin hall effect of tantalum, Science **336**, 555 (2012).

[28] T. V. P. Bliss and T. Lomo, Long-lasting potentiation of synaptic transmission in the dentate area of the unanaesthetized rabbit following stimulation of the perforant path, J. Physiol. **232**, 357 (1973).

[29] C. C. Bell, V. Z. Han, Y. Sugawara, and K. Grant, Synaptic plasticity in a cerebellum-like structure depends on temporal order, Nature **387**, 278 (1997).

[30] G. Bi and M. Poo, Synaptic modifications in cultured hippocampal neurons: Dependence on spike timing, synaptic strength, and postsynaptic cell type, J. Neurosci. **18**, 10464 (1998).

[31] B. Gao, Y. Bi, H.-Y. Chen, R. Liu, P. Huang, B. Chen, L. Liu, X. Liu, S. Yu, H.-S. Philip Wong, and J. Kang, Ultra-low-energy three-dimensional oxide-based electronic synapses for implementation of robust high-accuracy neuromorphic computation systems, ACS Nano **8**, 6998 (2014).

[32] H. Markram, J. Lübke, M. Frotscher, and B. Sakmann, Regulation of synaptic efficacy by coincidence of postsynaptic APs and EPSPs, Science **275**, 213 (1997).

[33] S. Boyn, J. Grollier, G. Lecerf, B. Xu, N. Locatelli, S. Fusil, S. Girod, C. Carrétéro, K. Garcia, S. Xavier, J. Tomas, L. Bellaiche, M. Bibes, A. Barthélémy, S. Saïghi, and V. Garcia, Learning through ferroelectric domain dynamics in solid-state synapses, Nat. Commun. **8**, 14736 (2017).

[34] C. Wu, T. W. Kim, H. Y. Choi, D. B. Strukov, and J. J. Yang, Flexible three-dimensional artificial synapse networks with correlated learning and trainable memory capability, Nat. Commun. **8**, 752 (2017).

[35] D. Sarkar, J. Tao, W. Wang, Q. Lin, M. Yeung, C. Ren, and R. Kapadia, Mimicking biological synaptic functionality with an indium phosphide synaptic device on silicon for scalable neuromorphic computing, ACS Nano **12**, 1656 (2018).

[36] S. Kyungah, I. Kim, S. Jung, M. Jo, S. Park, J. Park, J. Shin, K. P. Biju, J. Kong, K. Lee, B. Lee, and H. Hwang, Analog memory and spike-timing-dependent plasticity characteristics of a nanoscale titanium oxide bilayer resistive switching device, Nanotechnology **22**, 254023 (2011).

[37] T. V. P. Bliss and G. L. Collingridge, A synaptic model of memory: Long-term potentiation in the hippocampus, Nature **361**, 31 (1993).

[38] S. J. Martin, P. D. Grimwood, and R. G. M. Morris, Synaptic plasticity and memory: An evaluation of the hypothesis, Annu. Rev. Neurosci. **23**, 649 (2000).

[39] T. Ohno, T. Hasegawa, T. Tsuruoka, K. Terabe, J. K. Gimzewski, and M. Aono, Short-term plasticity and long-term potentiation mimicked in single inorganic synapses, Nat. Mater. **10**, 591 (2011).

[40] S. G. Hu, Y. Liu, T. P. Chen, Z. Liu, Q. Yu, L. J. Deng, Y. Yin, and S. Hosaka, Emulating the Ebbinghaus forgetting curve of the human brain with a NiO-based memristor, Appl. Phys. Lett. **103**, 133701 (2013).

[41] Y. Li, Z. Wang, R. Midya, Q. Xia, and J. J. Yang, Review of memristor devices in neuromorphic computing: Materials sciences and device challenges, J. Phys. D: Appl. Phys. **51**, 503002 (2018).

[42] P. Yao, H. Wu, B. Gao, S. B. Eryilmaz, X. Huang, W. Zhang, Q. Zhang, N. Deng, L. Shi, H.-S. Philip Wong, and H. Qian, Face classification using electronic synapses, Nat. Commun. **8**, 15199 (2017).

[43] I. Gupta, A. Serb, A. Khiat, R. Zeitler, S. Vassanelli, and T. Prodromakis, Real-time encoding and compression of neuronal spikes by metal-oxide memristors, Nat. Commun. **7**, 12805 (2016).

[44] A. Serb, J. Bill, A. Khiat, R. Berdan, R. Legenstein, and T. Prodromakis, Unsupervised learning in probabilistic neural networks with multi-state metal-oxide memristive synapses, Nat. Commun. **7**, 12611 (2016).

[45] M. M. Shulaker, G. Hills, R. S. Park, R. T. Howe, K. Saraswat, H. S. P. Wong, and S. Mitra, Three-dimensional integration of nanotechnologies for computing and data storage on a single chip, Nature **547**, 74 (2017).